Supersonic gas injector for plasma fueling in the National Spherical Torus Experiment

V. A. Soukhanovskii,[a],[*] W. R. Blanchard,[b] J. K. Dong,[b] R. Kaita,[b],[†]

H. W. Kugel,[b],[†] J. E. Menard,[b] T. J. Provost,[b] R. Raman[c]

A. L. Roquemore,[b],[†] and P. Sichta[b]

[a] *Lawrence Livermore National Laboratory, Livermore, CA, USA*
[b] *Princeton Plasma Physics Laboratory, Princeton, NJ, USA*
[c] *University of Washington, Seattle, WA, USA*

[*]E-mail: vlad@llnl.gov
[†]Retired

Number of pages: 31

Number of tables: 0

Number of figures: 17

Abstract

A supersonic gas injector (SGI) has been developed for fueling and diagnostic applications on the National Spherical Torus Experiment (NSTX). It is comprised of a graphite converging-diverging Laval nozzle and a commercial piezoelectric gas valve mounted on a movable probe at a low field side midplane port location. Also mounted on the probe is a diagnostic package: a Langmuir probe, two thermocouples and five pick-up coils for measuring toroidal, radial, vertical magnetic field components and magnetic fluctuations at the location of the SGI tip. The SGI flow rate is up to 1.75 x 10^{22} particles/s (250 Torr l / s), comparable to conventional NSTX gas injectors. The nozzle operates in a pulsed regime at room temperature and a reservoir gas pressure up to 5000 Torr. The deuterium jet Mach number of about 4 and the divergence half-angle of 5° - 25° have been measured in laboratory experiments simulating NSTX environment. Reliable operation of the SGI and all mounted diagnostics at distances 1-20 cm from the plasma separatrix has been demonstrated in NSTX experiments. The SGI has been used for fueling of ohmic and 2-4 MW NBI heated L- and H-mode plasmas. Fueling efficiency in the range 0.1 - 0.3 has been obtained from the plasma electron inventory analysis. SGI-fueling based plasma discharge scenarios enabling better density control have been developed.

I. INTRODUCTION

Gas injection at the plasma edge is universally used for fueling of high-temperature plasmas in present day magnetically confined fusion (MCF) devices. Its well-known shortcomings include a low fueling efficiency, in the range 0.01 - 0.2, and gas loading of in-vessel surfaces that may lead to uncontrolled fueling of plasma by out-gassing and recycling. The fueling efficiency is defined in a global sense as $\eta = (dN_i/dt) \ \Gamma_{gas}^{-1}$, where N_i is the confined particle inventory, and Γ_{gas} is the gas injection rate. Despite the shortcomings, the gas injection technique is likely to be used in future long-pulse experimental reactors, such as ITER [1, 2, 3], to complement other fueling techniques - the cryogenic pellet injection, energetic neutral beam injection (NBI), and compact toroid injection. A variation of the gas injection technique - a high-pressure low-divergence supersonic gas jet, also referred to as a supersonic molecular beam - was considered in early days of fusion research [4], and later implemented on a number of high-temperature MCF devices [5, 6, 7, 8, 9, 10, 11, 12, 13, 14, 15, 16, 17] .The gas jet is formed by a nozzle attached to a gas valve capable of pulsed operation on a fast ($\sim$ ms) time scale. A higher fueling efficiency of 0.3-0.6 and a reduced gas-wall interaction, and therefore a lower wall saturation limit have been observed in L-mode plasma experiments in limiter tokamaks. In divertor tokamak experiments with the supersonic gas jet, a fueling efficiency of 0.1-0.3 has been reported.

A supersonic gas injector (SGI) has been developed on the National Spherical Torus Experiment (NSTX) [8]. Physics research with the SGI aimed at 1) fueling optimization in long-pulse high-performance H-mode plasmas and H-mode pedestal fueling studies, 2) studies of the fueling efficiency and penetration of the high-pressure supersonic gas jet in divertor configurations, 3) studies of the synergy of efficient SGI fueling and wall pumping provided by lithium coatings, the latter being a major Boundary Physics research thrust on NSTX [18]. Typically, plasma fueling in NSTX was accomplished by injecting deuterium or helium through several piezoelectric or pneumatic valves with injection rates up to 100-150 Torr l / s, and a fueling efficiency of ≤ 0.1 [19, 20]. The SGI has been used for fueling of ohmic and 2 - 6 MW NBI-heated L- and H-mode plasmas in NSTX. The SGI was designed to operate in a long pulse steady-state mode, injecting gas at a flow rate similar to conventional gas injectors, typically $N_{pulse} \simeq (0.1 - 0.5) \times N_i$. This distinguished it from the other supersonic gas injectors studied on other MCF plasma devices [6, 7, 10] and designed to inject gas in massive quantities $\Delta N_{pulse} \simeq (0.2 - 0.9) \times N_i$ in milliseconds, leading to

localized cooling of the plasma edge or confinement degradation.

This paper describes the design and technical implementation of the SGI on NSTX. The paper is organized as follows. Section II describes conceptual considerations applied to the SGI design. The initial implementation and results with the SGI operated at D_2 pressures $P \leq 2500$ Torr are described in Section III. Section IV presents the details of implementation and result with the SGI upgraded to a higher has reservoir pressure $P \leq 5000$ Torr. Section V included the procedures developed for spatial calibrations of the movable SGI head, and gas flow rate calibrations.

II.   SUPERSONIC GAS INJECTOR AND NOZZLE DESIGN CONSIDERATIONS

In the tokamak, supersonic gas jet operation principles are based on diverse physics fields: gas-dynamics, compressible fluid mechanics, neutral gas transport, and magnetized plasma physics. An expansively cooled supersonic gas jet is obtained by expanding room-temperature or cooled gas from a high pressure reservoir through a nozzle into vacuum. In the tokamak, the gas jet interacts with low-density plasmas: it penetrates through the plasma scrape-off layer perpendicular to the magnetic field lines, ionizes in the separatrix region and creates a localized high pressure plasma region. This plasmoid region expands along field lines, locally cooling and fueling the edge plasma. The radial propagation of the high-pressure gas jet through the edge plasma is determined to the first order by the fluid force balance, mainly by the relative magnitude of the plasma (magnetic and kinetic) pressure and the gas jet impact pressure. The high pressure gas jet undergoes molecular and atomic (charge exchange, ionization) reactions as it propagates through the scrape-off layer plasma, retaining a neutral core shielded by an ionizing layer. The gas jet density plays a critical role in the penetration mechanism, as has been demonstrated by analytic and numerical modeling [21, 10, 22]. However, a deep penetration may be inhibited by a high-density ionizing plasmoid that rapidly develops in front of the gas jet and blocks the jet from further penetration.

The nozzle is an important part of the SGI. In principle, gas injection through any expansion (nozzle) can produce a supersonic jet if a ratio between the nozzle reservoir pressure and the background pressure, P_0/P_{bg}, is adequate as determined by the compressible fluid mechanics [23]. However, it is the nozzle geometry that determines supersonic jet properties, particularly the Mach number M and the degree of clustering (and condensation) of gas molecules.

The significance of a high Mach number is that the Mach focusing of the gas flow leads

to a formation of a low divergence high pressure jet. The supersonic jet velocity is $u = Mc = M\sqrt{\gamma kT/m}$, c is a local speed of sound, and γ is the specific heat ratio. The static temperature T in a compressible flow, however, is reduced according to $T/T_0 = (1 + \frac{\gamma-1}{2}M^2)^{-1}$, where T_0 is the stagnation temperature, so that the terminal velocity is $u_{max} = \sqrt{\frac{2\,\gamma}{\gamma-1}\frac{kT_0}{m}}$. The particle velocity distribution in the jet is described by a drifting narrowed Maxwellian distribution with the drift velocity u. Thus, the jet velocity u is only a factor of $2-3$ greater than the thermal gas velocity $v_{th} = \sqrt{3kT_0/m}$. Clustering of a molecular gas may increase the jet density by orders of magnitude in comparison with pure molecular or atomic gas jet. It is characterized by the empirical Hagena parameter [24] for given nozzle and jet parameters. These two properties are believed to be crucial for tokamak plasma fueling applications.

Four axisymmetric nozzle shapes are commonly used for making high quality supersonic gas jets: a converging nozzle (free jet), a converging-diverging Laval nozzle, a converging-diverging conical nozzle, and an aerospike (plug) nozzle (e.g., [8]). In comparison with a simple converging nozzle [25], a shaped Laval nozzle can produce a highly uniform flow with constant Mach number, temperature, and density - the conditions favorable for molecular condensation. A higher flow intensity can be obtained with a lower pressure ratio P_0/P_{bg} in a contoured (Laval) nozzle avoiding problems associated with normal Mach disk shocks. The Laval nozzle shape must be properly calculated to optimize the isentropic flow core and minimize the thickness of the boundary layer. This is usually done using the method of characteristics or computational fluid dynamics methodology based on numerical solution of the Navier-Stokes equations [23]. The nozzle design is based on an established flow with steady-state parameters. For tokamak fueling applications, pulsed gas jet operation may be desirable: hence, the finite flow settle time may limit the minimum pulse length.

III.   INITIAL SGI IMPLEMENTATION ON NSTX.

III.A.   Supersonic gas injector design and characterization

The SGI design incorporates several engineering and physics requirements: operational and vacuum autonomy, least interaction with NSTX machine operation and maintenance cycle, radial translation capability, gas throughput and diagnostic needs. For these reasons the SGI and several edge diagnostics are placed on a radially moving remotely controlled probe. The probe is mounted
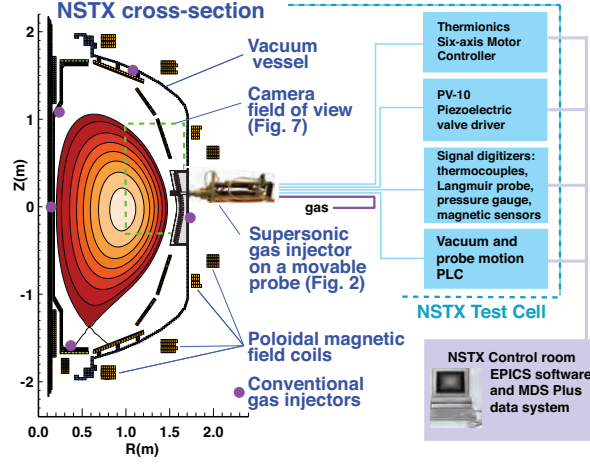
Fig. 1. Supersonic gas injector placement on NSTX and a block diagram of SGI control elements.

on a stand, and enters the NSTX vacuum vessel through a standard 4" diameter port at a low field side (LFS) midplane location, at a distance 0.16 m above the midplane. The port is equipped with a machine vacuum interface valve. Shown in Fig. 1 is the SGI placement and control infrastructure schematic. Fig. 2 shows photographs of the SGI probe and the SGI head assembly. A ceramic break is used to isolate the probe electrically from the NSTX vacuum vessel potential. The SGI includes a small graphite nozzle, a commercial piezoelectric gas valve and the gas-handling hardware. The diagnostic package is comprised of a Langmuir probe, two thermocouples, and an Edge Magnetic Sensor (EMS) with five magnetic pick-up coils. The diagnostics and the valve with the nozzle are enclosed in a probe head covered by a protective shroud. The shroud is made of carbon fiber composite and ATJ graphite because of their low sputtering coefficient. All materials used in the SGI are ultra high vacuum compatible. The head is mounted on the Thermionics ZC-450 movable probe as shown in Fig. 2. The probe stroke is 24 inches, with a step size 0.0005 inches and a travel rate up to 15 in/sec. A 0.5 inch flexible gas line, a 0.25 inch OD gas line and electric cables are routed along the stand and connected to the SGI through vacuum electrically isolated feed-throughs. A 0.5 inch OD gas line and cables are mounted in vacuum inside the flexible probe bellows. The gas delivery lines are designed to handle high-pressure flowing gas in a viscous regime with minimum boundary layer effects for a typical SGI deuterium pressure up to $P_0 \leq 2500$ Torr. The gas delivery system includes a Sensotec Model TJE 5821-01 absolute pressure transducer for plenum pressure measurements before and after an injection pulse and a fill isolation valve
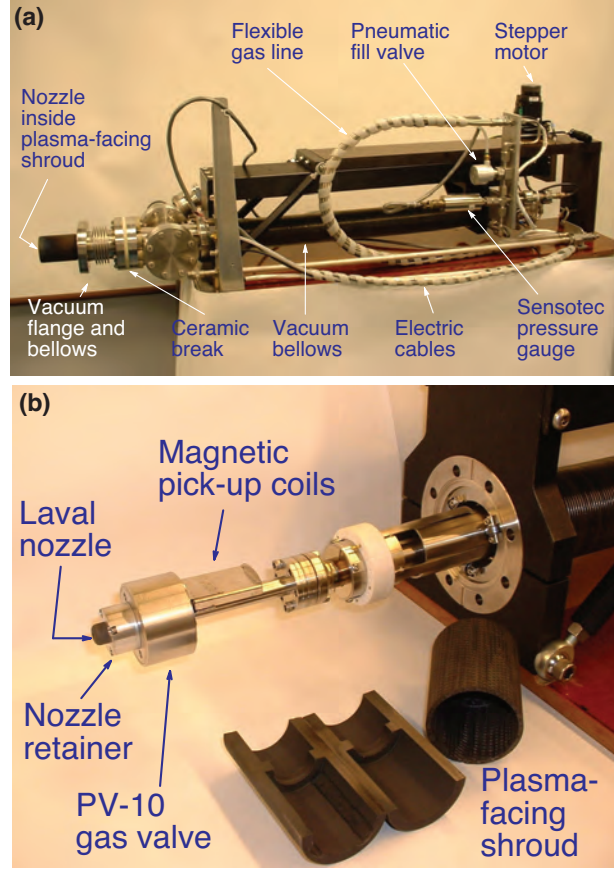
Fig. 2. A photograph of the SGI probe on a mounting stand (a) and the SGI head assembly (b).

actuated by compressed air. The SGI gas line is connected to the NSTX Lower Dome and Inner Wall gas system [20] which uses standard gas bottles with a maximum regulator pressure of 2500 Torr imposed by hardware limits. The electric cables mounted inside the probe bellows are low-voltage signal cables with an exception of a SGI piezoelectric valve driver cable. The Veeco PV-10 piezoelectric precision leak valve with a throat diameter 0.02 inches is used in the SGI. The valve operating temperature range is $0-50$ °C. The valve characteristic opening time is 1-2 ms as verified by laboratory measurements [8]. Whereas the flow rate is proportional to the applied voltage in the range between 60 and 150 V, the valve is always operated at 150 V. The SGI plenum pressure variation is used to alter the flow rate. The flow rate calibration is discussed in Section V.

As mentioned above, several diagnostics are densely packed under the protective shroud around and behind the gas valve. Integrated into the front surface of the shroud are a single Langmuir probe, a thermocouple, and two magnetic pick-up coils (Fig. 3). The Langmuir probe is a flush-mounted type graphite probe with a 0.069 inch diameter tip. It is similar to the NSTX
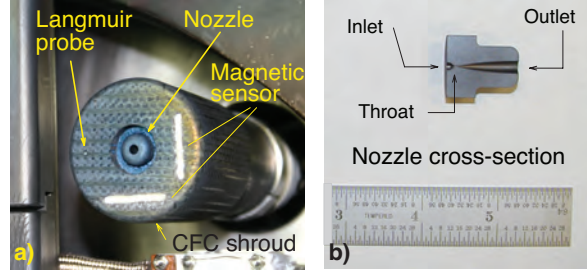
Fig. 3. Photographs of the SGI probe head inside the NSTX vacuum vessel (a) and the Laval nozzle (b). A flush-mount Langmuir probe tip and magnetic pick-up coil slots are visible on the SGI head.

divertor tile probes used to determine the scrape-off layer plasma potential, particle flux and with proper analysis, plasma temperature and density. The probe saturation current I_{sat} value in the tens of milliampers is obtained when the probe power supply voltage is swept between -50 V and 50 V. The thermocouples are used to monitor the shroud and the gas valve temperature during plasma operations. Two pick-up coils are mounted in slots on the front surface of the CFC shroud. Their spatial orientation enables measurements of the vertical B_z and toroidal B_t magnetic field components with a proper calibration. Three pick-up coils are mounted in a small shielded box behind the gas valve. Two of them are designed to measure radial B_r and vertical B_z magnetic field components while the third, Mirnov, coil is for edge magnetic fluctuation measurements.

The Thermionics probe is equipped with an encoder and a 6-axis stepper motor controller (SMC). The SMC is mounted in a rack in the NSTX Test Cell. The EPICS software is used to communicate with the vacuum programmable logic control elements, such as the probe limit switches, vacuum and gas valves, and control the SMC remotely using its RS-232 port. The software is executed on an NSTX Engineering Network computer safeguarded by a firewall computer, and runs from a terminal in the NSTX Control Room. The EPICS control software will be described in more detail in Section IV.

A converging-diverging Laval nozzle geometry (Fig.3 (b)) has been used in the SGI [8]. The geometry was obtained by scaling down by a factor of 60 a large wind tunnel nozzle operated in air ($\gamma = 1.401$) at $P = 1$ atm and $M = 8$ [26]. The nozzles were machined from graphite using the electrical discharge machining technique by by MWI, Inc. [27]. The nozzle throat diameter is $d = 0.01$ inches, the inlet diameter is 0.087 inches, and the exit diameter is 0.015 inches. The dimensional tolerance are ± 0.0025 inches, verified by precision measurements of one nozzle cut in half for quality control purposes. The nozzle is 0.92 inches long.

Nozzle characteristics and performance in a pulsed regime were evaluated in a laboratory setup that simulated the tokamak environment: the SGI injected gas pulses of 1 - 50 ms duration into a 50 liter vacuum tank with a background pressure $P_b = 10^{-4}$ Torr, similar to the neutral pressures measured in NSTX [8].The goal of the characterization was to measure the gas injection rates, and to evaluate the gas jet profile, the flow Mach number, velocity, temperature and density. A local Mach number was obtained under the assumption of isentropicity from the Rayleigh - Pitot law using the pressure measurements upstream and downstream of the shock formed in front of the pressure transducer immersed in the flow:

$$\frac{P_i}{P_0} = \left(\frac{(\gamma+1)\,M^2}{(\gamma-1)\,M^2+2}\right)^{\gamma/(\gamma-1)}\left(\frac{\gamma+1}{2\gamma M^2-(\gamma-1)}\right)^{1/(\gamma-1)} \tag{1}$$

The impact (stagnation) pressure P_i was measured on axis and the flow static pressure P_0 was measured in the SGI plenum [23]. Two identical nozzles labeled PN-1 and PN-2 were used in measurements with three gases: hydrogen, deuterium, and helium.

Shown in Fig. 4 are the measured gas jet impact pressure profiles obtained at $P_0 \simeq 1000$ Torr corresponding to the injection rate of 65 Torr l /s. The profiles were measured at different axial distances z from the nozzle exit. The jet profile was found to be insensitive to the background pressure in the range $10^{-5} < P_b < 100$ Torr, consistent with the notion that the optimal background pressure for a supersonic expansion is equal to the static flow pressure. The impact pressure profiles of hydrogen and deuterium jets were found to be similar, since the heat capacity ratios γ are 1.41 and 1.399, respectively. The central impact pressure of helium was smaller. Unlike the diatomic H_2 and D_2 molecules helium is a monatomic gas with $\gamma = 1.63$. The deduced Mach number at the nozzle exit was about 4 for hydrogen or deuterium, and about 6 for helium. When the deuterium pressure P_0 was lowered below 600 Torr, the ratio P_0/P_i sharply decreased as the flow approached sonic conditions. While the gas jet maintained its sharp density gradient for at least 120 mm along the axial distance z, the measured central pressure sharply decreased at about 10 mm from the nozzle exit. This could be due to the flow underexpansion resulting from the improper scaling of the nozzle. From the isentropic flow relations one could estimate the jet core diameter corresponding to $M \simeq 4$: $A_*/A|_{M=4} \simeq 10$, from which $d_{core} \simeq 0.7$ mm was obtained. The boundary layer appeared to be very thick, consistent with the measured profiles. The boundary layer thickness of the original Laval nozzle was measured to be 11.4 mm [26]. If it is scaled down by 60, the
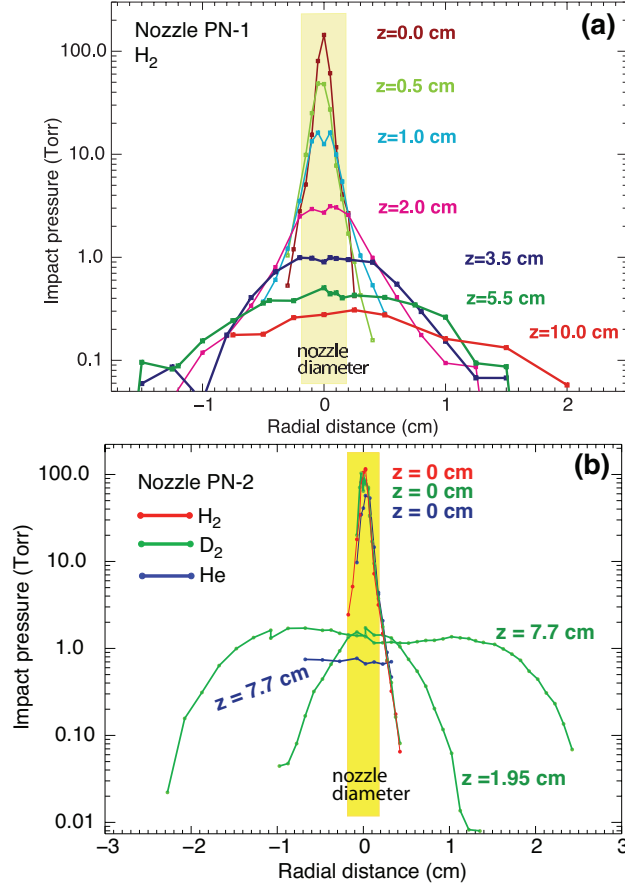
Fig. 4. Measured jet impact pressure profiles at different axial distances z from the nozzle exit: (a) nozzle PN-1 used with hydrogen; (b) nozzle PN-2 used with hydrogen, deuterium, and helium.

boundary layer of about 0.2 mm is obtained, a factor of 8 smaller than the one inferred from the measurements. The jet divergence half-angle was found to be $\theta_{1/2} \simeq 6 - 12°$. Using the isentropic relations between stagnation and static quantities [23], the density at the jet exit is estimated to be $\rho \leq 10^{18}$ cm^{-3}, and the temperature to be $T \geq 70$ K. The nozzle Reynolds number is $Re \simeq 6000$. The parameters discussed above indicate that the NSTX gas jet was not in the regime favorable for molecular cluster formation.

III.B.   Performance on NSTX

Initial experiments on NSTX focused on commissioning the SGI and the diagnostics, and studying the interaction of the supersonic gas jet with edge plasmas.

Deuterium pulses of 50-500 ms duration were injected in ohmically heated and NBI-heated L- and H-mode plasmas. In ohmically heated L-mode plasmas, the SGI head was brought as
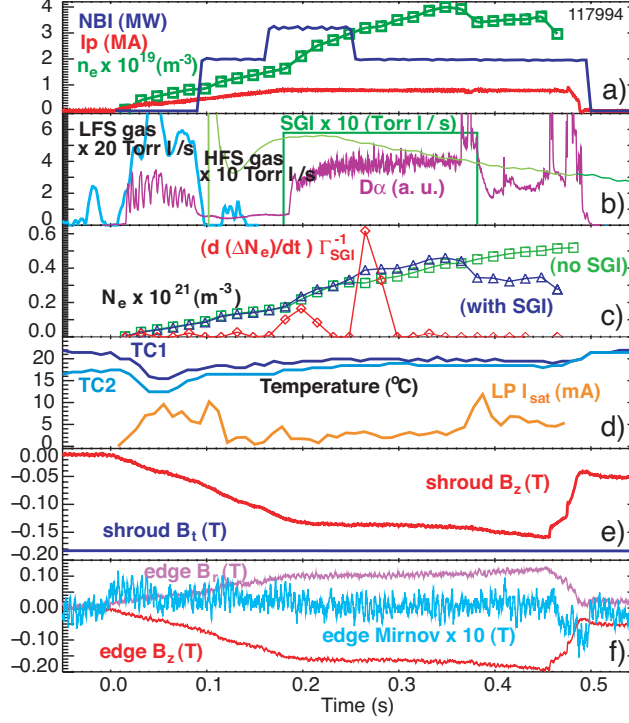
10

Fig. 5. Time traces of a representative SGI-fueled H-mode discharge. (a) Plasma current I_p, NBI power, line-averaged density $\bar{n}_e$, (b) Midplane D_α emission, gas flow rates for the low field side (LFS), high field side (high field side) injectors and SGI, (c) Total electron inventories for this shot and a shot without SGI, and the SGI fueling efficiency, (d) Shroud TC1 and gas valve TC2 thermocouple temperatures and Langmuir probe I_{sat}, (e) Shroud coil sensor traces of B_t and B_z, (f) edge coil sensor traces of B_r, B_z and magnetic fluctuations (Mirnov).

close as 1 cm to the plasma separatrix without any disruptive effects on the plasma or SGI head overheating. The plasma separatrix position was inferred from the magnetic equilibrium reconstruction code EFIT [28]. However, in NBI-heated plasmas the SGI head interacted with lost orbit energetic particles as soon as it cleared a limiter (a graphite surface in the midplane used for radio-frequency antenna protection). The resulting recycling and carbon flux from the SGI head caused a confinement degradation in H-mode plasmas (sometimes leading to H-L transitions), as well as disruptive MHD activity. Based on this experience, the SGI was always positioned in the shadow of the limiter at a distance 6-12 cm from plasma separatrix in NBI-heated discharges.

Typical time traces from diagnostics characterizing the plasmas and SGI are shown in Fig. 5. The waveforms are from a representative 2-4 MW NBI-heated H-mode plasma discharge fueled by the inner wall (high field side - high field side) gas injector. An SGI pulse of 200 ms duration was added starting at 0.18 s with a flow rate $\simeq 55$ Torr l /s. The SGI remained at a distance 8 - 13 cm from the plasma throughout the pulse duration. The SGI injection was clearly visible
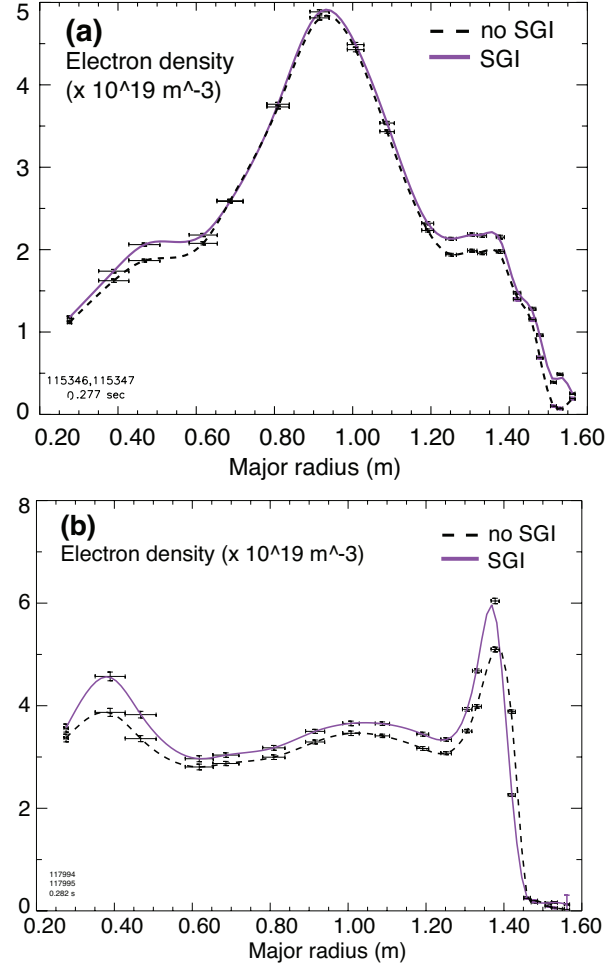
Fig. 6. Electron density profiles measured by the laser Thomson scattering system in (a) L-mode discharges and in (b) H-mode discharges with and without SGI fueling.

in the visible deuterium Balmer-α (D_α) emission waveform. Two inflections are seen on the line-integrated density $\bar{n}_e$ and the total electron inventory N_e time traces: the first one occurs at the inner wall gas injection onset time, and the second at the time of the SGI gas injection and an L-H transition onset. In order to calculate the SGI fueling efficiency, fueling contributions from other gas injectors, recycling and impurities must be taken into account. A difference between the total electron inventories ΔN_e of two consecutive discharges with and without an SGI pulse can be used to approximate the plasma particle content due to the SGI. The fueling efficiency can be taken as $(d\,\Delta N_e/dt)\Gamma_{SGI}^{-1}$, where Γ_{SGI} is the SGI flow rate. The total electron inventory N_e was obtained by volume-integrating the flux surface averaged Thomson scattering n_e profiles for each time point. Fueling efficiency between 0.1 and 0.3 has been inferred in this manner.
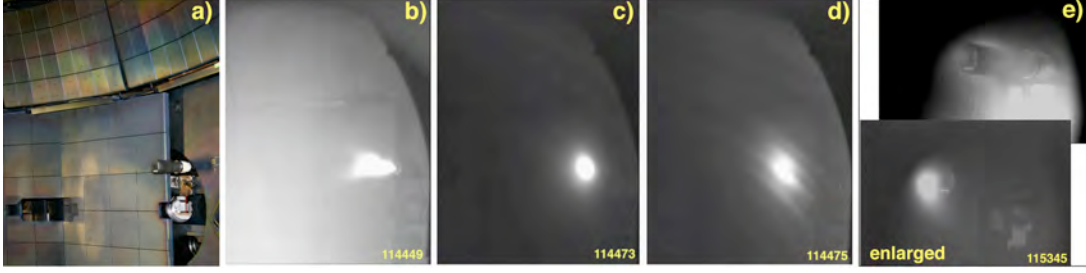
Fig. 7. Fast camera imaging of the SGI and deuterium gas jet interaction with edge plasmas. (a) The SGI head is inside the NSTX vacuum vessel at a radial position used for plasma fueling; light emission from a D_2 gas jet interacting with (b) a plasma with a wide scrape-off layer with nearly constant T_e and n_e; (c) 6 MW NBI-heated L-mode plasma; (d) 4 MW NBI-heated H-mode plasmas. (e) Close-up images of the SGI heat interacting with SOL plasmas.

The SGI diagnostic package has been commissioned and used in several experiments to study the SGI performance and edge plasma characteristics. Shown in Fig. 5 are signal traces from the SGI probe diagnostics. Both thermocouples usually measured room temperatures throughout a plasma pulse. The Langmuir probe saturation current I_{sat} time trace showed weak increase (if any) in the SOL particle flux during the SGI pulse. The EMS was used in the poloidal field only start-up experiments to monitor field null formation, and during SGI pulses to monitor edge magnetic field perturbations, and edge MHD activity. The EMS signal traces shown in Fig. 5 used preliminary magnetic calibration factors. Hence, we conclude that the SG gas jet does not produce any adverse local perturbations of the edge plasma at the gas flow rates used.

Plasma density profiles measured with and without the SGI fueling clearly showed additional particle (density) deposition at the edge. Shown in Fig. 6 are the electron density profiles measured by the laser Thomson scattering system [29, 30] in L-mode discharges (a) and in H-mode discharges (b). In each plot, density profiles from two discharges with identical heating and fueling (except the SGI) are compared. The n_e profiles indicate that the edge L-mode density, as well as the pedestal region (H-mode "ear") height and possibly width undergo changes as as a result of SGI fueling whereas the core plasma often remains unaffected.

Fast camera imaging was used to monitor gas jet formation, evolution, and the SGI head and jet interaction with the SOL plasma. Shown in Fig. 7 are photographs of the SGI head (that includes the nozzle enclosed in the shroud) and the visible light from the deuterium gas jet interaction with different types of plasma. The data was recorded by a Canadian Photonics camera operated at 1 ms frame rate and a line of sight forming a 48° angle with the SGI axis. Gas jet

13

divergence of 40-60° degrees and the formation of a high-density region have been inferred from the images of a bright localized light region during SGI gas puffing. The emission comes mostly from the deuterium Balmer series lines in the visible range ($D_\alpha, D_\beta, ...$). The estimated jet divergence was consistent with the measured pressure profiles described in Section III A. Of note is the jet image shown in Fig. 7 (b) that was obtained in the end of a plasma discharge when the plasma was moving inward. A thick quasi-steady-state SOL region was formed outside with nearly constant $T_e = 3$ eV and $n_e = 2 - 2.5 \times 10^{18}$ m^{-3} as measured by the laser Thomson scattering diagnostic. These plasma conditions favored atomic deuterium emission and led to a full jet visualization, confirming that the SGI formed a collimated jet. However, in a typical plasma SOL with strong n_e and T_e radial gradients, the emission region was usually round and small. The 5-10 cm light region was typically elongated along the field lines. The plasmoid was located from 0.5 to 6 cm outside of the separatrix. If the ionization took place in the same region where the electron impact excitation and optical emission took place, it would mean that the SGI ionization source was also located in the SOL region. Plasma turbulence filaments ("blobs") and ELMs freely traversed through the plasmoid possibly affecting its fueling characteristics. The SGI emission region size was typically much smaller than a light-emitting cloud produced by a conventional gas injector.

IV. HIGH PRESSURE UPGRADE IMPLEMENTATION ON NSTX

The SGI was successfully commissioned and used to fuel L- and H-mode plasmas in its initial operation phase. Good progress was also made toward a SGI-fueled controlled density H-mode plasma scenario. Most NSTX H-mode plasma scenarios used the high filed side (inner wall) gas injector with uncontrolled dynamic fueling rate, which was believed to be a factor contributing to uncontrolled density rises in NSTX [31]. The SGI-fueled H-mode plasma scenario was able to use the high filed side gas injector with a significantly reduced flow rate (up to 20). As a result, comparable or slightly higher core and pedestal densities were obtained, with 5 - 15 % reduction of core and pedestal temperatures, and a change in the ELM character from Type I and small, Type V ELMs to Type III ELMs. The SGI was operated with deuterium in these experiments as the gas delivery configuration was common with the high filed side gas injection system. These initial results motivated a number of upgrades of the SGI apparatus, its gas delivery system, and its control elements, namely: 1) to increase the available plenum pressure to 5000 Torr (100 PSIA),

thus increasing the jet pressure and the flow rate, 2) to increase the plenum pressure volume, 3) to change the gas delivery system to allow for injection of gases other than deuterium, and 4) to enable multi-pulse capability for better fueling control in one plasma discharge.

Increasing the SGI plenum pressure from 2500 Torr to 5000 Torr required a number of modifications to mechanical and electrical gas system components. Various system aspects were considered during the SGI-2 design: gas tube routing around the NSTX vacuum vessel, high-pressure gas pump-out solutions, remote measurement and control of the SGI-2 plenum pressure, electrical isolation and proper grounding of the SGI hardware, and overall system control. Characterizing and understanding the nozzle and valve performance at higher pressures were also considered a high priority element of the SGI-2 upgrade work. This Section describes the upgrades and results obtained with SGI upgrade referred henceforth as SGI-2.

IV.A.   SGI and gas delivery system modifications

The SGI-2 design retained the existing hardware components that were rated for a 5000 Torr (665 kPa, 95.5 PSIA) operation. Shown in Fig. 8 are the photographs of the SGI and SGI-2 apparatuses. In the SGI-2 design, all original 12.5 mm OD stainless steel gas lines and joints were retained. At pressures $P \leq$ 5000 Torr, the gas flow is in the viscous (Poiseuille) flow regime, where a viscous boundary layer effect due to flow shear at the wall is non-negligible. Because of the boundary layer the flow rate Q_m is a linear function of the pressure P even for sonic laminar pipe flows, deviating from the ideal Poiseuille flow regime ($Q_m \sim P^2$) [32]. The boundary layer thickness is independent of flow pressure once the flow reached the viscous regime. Therefore, the SGI-2 gas delivery system performance was expected to be similar at both 2500 Torr and 5000 Torr. A supersonic nozzle flow rate is also linearly proportional to plenum pressure. To reduce the effect of a flow rate reduction with a plenum pressure drop during SGI gas pulses in one plasma discharge, a larger gas reservoir was considered. Previously, when a plenum volume of 125 cc was used, a reduction in the flow rate by up to 10-15 % was observed. A new calibrated plenum volume of 150 cc (Fig. 8) was added to the system. The effective SGI-2 plenum volume, accounting for other changes, was estimated to be 250 cc. Several SGI components have been upgraded to high pressure-rated (100-200 PSIA) models. The upgraded components (highlighted in Fig. 8) included: CeramTech ceramic breaks (used for electric isolation), a flexible hose, an electric feedthrough, a
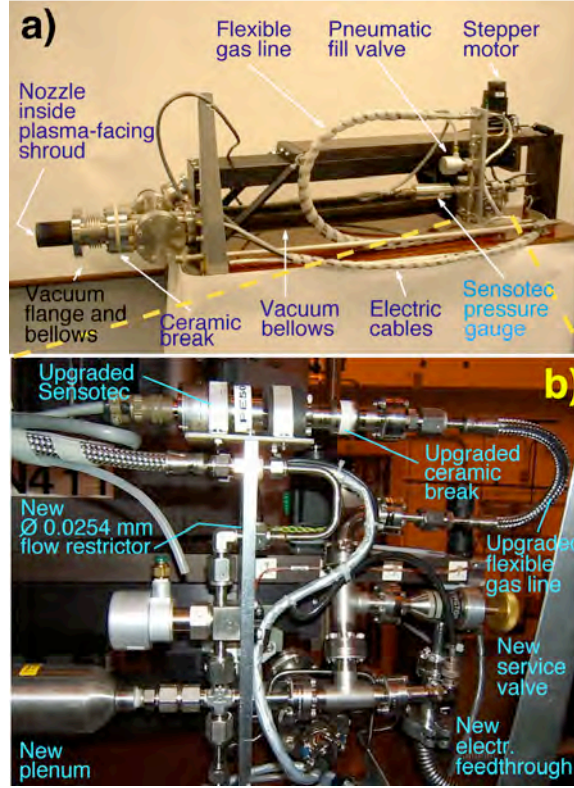
15

Fig. 8. Photographs of the supersonic gas injector (a) and an enlarged view of the upgraded SGI (b). Highlighted in light blue are the components upgraded to handle 100 PSIA pressure.

0.0254 mm ID orifice (serving as a flow restrictor), and a pressure transducer (Sensotec Model TJE AP122BR). The diagnostics mounted on the SGI head - the Langmuir probe, thermocouples, and magnetic pick-up coils - have not been modified.

Substantial changes were made to the SGI gas delivery system. The new system schematic is shown in Fig. 9. Previously, the SGI gas line was connected to the NSTX Lower Dome and Inner Wall (high field side) gas system [20]. Standard gas bottles with a maximum pressure of 2500 Torr imposed by hardware limits and limited by a gas regulator were used. The SGI-2 design goals required an independent high-pressure-rated gas delivery and pump-out system. A cost and labor effective solution was found: a gas delivery system of one of the existing (conventional) gas injectors was modified and connected to the SGI-2. Most of the existing hardware infrastructure, computer and PLC controls were retained. The upgrades included ceramic breaks, flexible bellows, and an addition of two new pneumatic isolation Nupro valves. Sensotec pressure transducers were replaced and a Baratron pressure gauge was added. On the gas cylinder end, upgrades involved
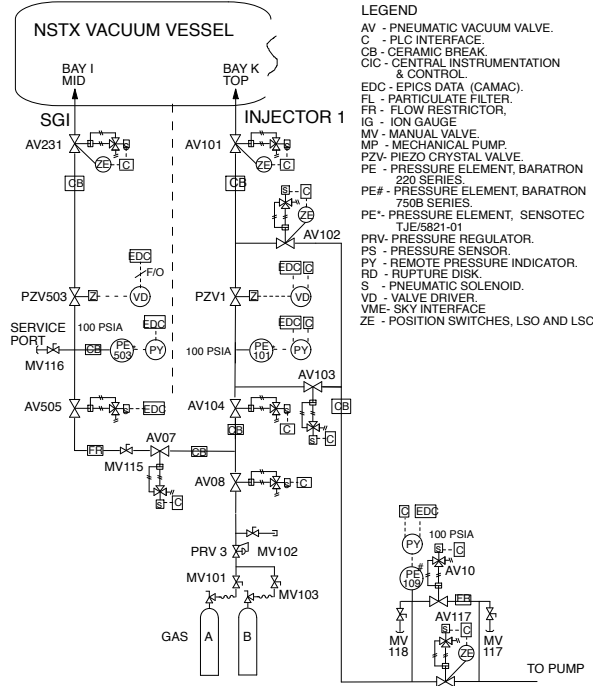
16

Fig. 9. A schematic of the SGI-2 gas delivery system.

replacing gas cylinder regulators by 200 PSIG rated models (Matheson Tri-Gas Model 3122 dual stage regulator). The pump-out system was modified to include a by-pass with a flow restrictor to avoid overloading the NSTX mechanical pump with high pressure gas. These changes are reflected in the SGI-2 gas delivery system shown in Fig. 9. The design enables filling the SGI-2 remotely (from a NSTX Control Room terminal) with any gas from gas bottle A, while operating the conventional gas injector (Injector 1) at a different pressure up to 5000 Torr with gas from bottle B.

The EPICS system [33] was previously used for SGI control, operation and programmable logic control (PLC) functions. Shown in Fig. 10 is the EPICS software interface used to operate and control the SGI-2. An EPICS software interface is run on a terminal in the NSTX control room. Computer controls and PLC functions and events were modified to reflect the hardware changes described above. A multi-pulse capability was also added: up to ten pulses could be enabled in one plasma discharge (compared to one SGI pulse per a plasma discharge previously). An SGI-2 operator specifies the radial location of the SGI-2 head, and executes the SGI-2 probe
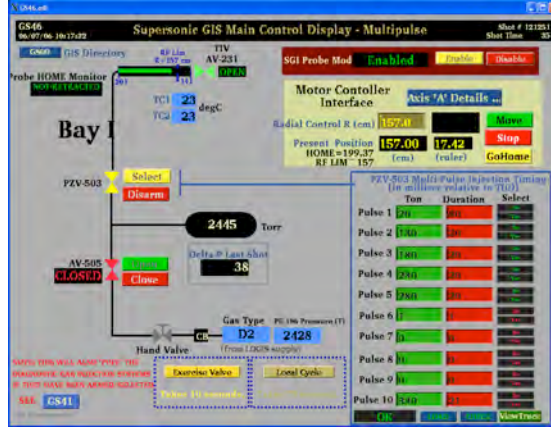
Fig. 10. EPICS software interface page used to operate and control SGI-2.

motion. The probe is usually kept at $R = 1.98$ m when unused, and at $R = 1.52 - 1.60$ m (several cm from plasma) during plasma operations. The operator also specifies the plenum fill pressure and the start times and durations for gas pulses. The fill and pump out functions of the gas delivery system are also controlled from the interface. The SGI-2 operation was synchronized with the NSTX discharge clock cycle. A manual pulsing capability for test or calibration purposes was also developed.

IV.B. Nozzle and valve characterization at high pressure

A converging-diverging Laval nozzle was used in the NSTX SGI and the laboratory characterization of the nozzle was descibed in Section III. Nozzle and piezoelectric valve performance at higher pressures were studied for the SGI-2. Measured flow rates were found to be linear functions of plenum pressure for a stand-alone Veeco PV-10 valve and for an assembly of the valve and nozzle, consistent with previously measured rates. At the deuterium plenum pressure of 2500 Torr, the SGI-2 flow rate was ~ 100 Torr l /s, while at 5000 Torr, the flow rate was approaching 200 Torr l / s. To characterize performance of a supersonic gas jet, impact pressure P_i measurements at the nozzle exit as a function of plenum (stagnation) pressure P_0 were performed with deuterium, helium and nitrogen (Fig. 11). Deuterium injection at rates $Q \leq 120$ Torr l / s was used in NSTX for fueling, whereas helium and nitrogen injection at rates $Q \leq 5 - 10$ Torr l / s could be used for diagnostic purposes, and in transport and radiative divertor experiments. The Mach number M_d inferred from the P_i measurements using the supersonic Rayleigh-Pitot law was about 4 for a full range of available P_0 pressures in deuterium, since the ratio P_0/P_i changed proportion-
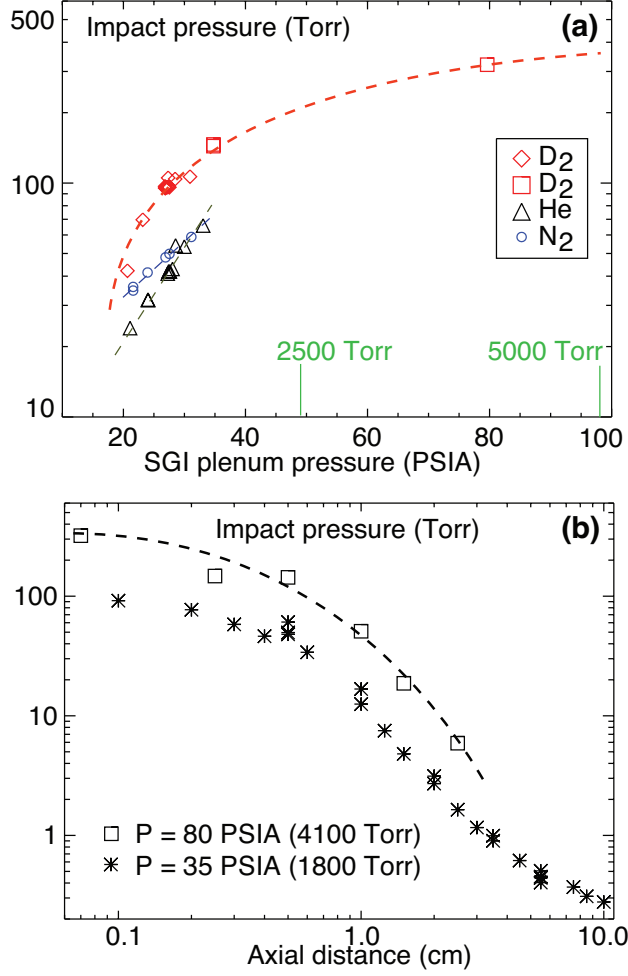
18

Fig. 11. (a) Supersonic gas jet impact pressure measured at the nozzle exit on axis as a function of plenum pressure for deuterium, helium and nitrogen. (b) Supersonic gas jet impact pressure measured along the axis. Lines are drawn to guide the eye.

ally with P_0. The Mach number M appeared to be slightly higher for helium and nitrogen at lower P_0 pressures. The observed independence of M from the plenum pressure P_0 was interpreted as confirmation of the supersonic flow regime: the boundary layer did not change significantly with pressure, and an isentropic jet core existed in a range of pressures. The increased plenum pressure range in SGI-2 led to a higher flow rate and a greater fueling flexibility. Before the upgrade, the SGI jet impact pressure was limited to about 30 kPa at the nozzle exit, and about 0.02 kPa at a distance 10 cm from the nozzle (Fig.4). The jet impact pressure in the SGI-2 at $P_0 = 4100$ Torr was several times higher (Fig. 11). The plasma pressure at the separatrix in NSTX was in the range $P = P_{kin} + P_{magn} \simeq 0.01 - 0.1$ kPa, suggesting (based on these hydrodynamic arguments) that the SGI-2 jet might be able to penetrate closer to the separatrix.
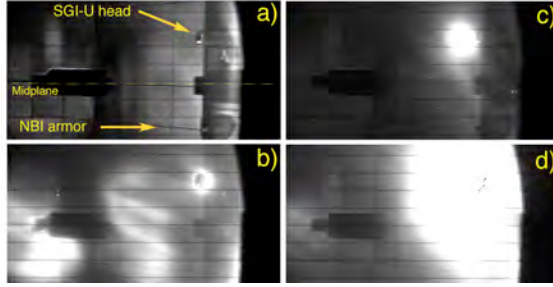
Fig. 12. Fast camera images of SGI-2 operation: (a) SGI-2 head in the vacuum vessel at $R = 157$ cm, (b) Plasma interaction with SGI-2 head during an MHD event, (c) D_α emission from high-pressure deuterium jet in the initial phase of injection, (d) D_α emission during high-pressure deuterium pulse (camera saturated).

IV.C. SGI-2 performance on NSTX

Fueling experiments have been carried out on NSTX to explore the higher pressure SGI-2 impact on plasma and fueling characteristics.

Fast framing camera images taken during SGI-2 operation at the highest plenum pressure (5000 Torr) showed a highly localized plasma-jet interaction region (Fig. 12). A bright localized light region was consistent with the measured jet divergence half-angle of $\theta = 6 - 25°$. Deuterium was injected in the L- and H-mode phases of a discharge. High-speed camera visualizations of the SGI-2 jet interactions with edge plasma qualitatively looked similar to the previous SGI observations shown in Fig. 7. However, the light intensity was much higher than previously observed (up to a camera saturation level), an indication of a higher jet density and possibly a higher penetration (i.e. emission at higher edge electron densities and temperatures).

The high-pressure SGI-2 injection did not lead to an H-L transition, as in previous SGI fueling experiments. Shown in Fig. 13 are the waveforms of a representative 4-6 MW NBI heated H-mode discharge. In this experiment, reduced high field side fueling was used (500 Torr plenum pressure vs 900-1200 Torr typically used). The SGI-2 was operated at a plenum pressure of 5000 Torr. The SGI-2 head was positioned at a major radius of 157 cm, about 5-10 cm from the plasma last closed flux surface (obtained from the EFIT equilibria reconstructions [28]. The H-mode transition occurred at 0.26 s, so that the first SGI-2 pulse was injected in the L-mode current ramp-up phase, while two subsequent pulses were in the H-mode phase of the discharge. The SOL density did not change during the SGI-2 pulses, while the inboard and outboard pedestal density increased, suggesting particle deposition in the edge/near-SOL region. The total electron inventory $N_e(t) = \int n_e dV$ also

increased during the SGI-2 pulses as evident from its time derivative dN_e/ dt. However, the edge particle containment time appeared to be low ($\tau \leq 10$ ms) as the deposited particles were quickly lost from the plasma. The plasma n_e, T_e profiles shown in Fig. 13 (e) and (f) indicated that a SGI-2 pulse in the H-mode phase led to a rapid increase in the pedestal density by 10-30 %, and a small pedestal temperature decrease. The gas jet fueling efficiency $\eta = (d \, \Delta N_e/dt)\Gamma_{SGI}^{-1}$ estimated from the total electron inventory N_e derivative and the SGI-2 injection rate, was in the range 0.1 - 0.3. It was comparable to the SGI fueling efficiency obtained at lower plenum pressures. This result may imply that the present supersonic gas jet characteristics are at a physical fueling limit, and a higher fueling efficiency w.r.t. a conventional gas injection is mostly due to a geometric focusing effect.

Previous work on H-mode fueling optimization in NSTX led to a fueling scenario with the high field side gas injection that facilitated H-mode access [34]. However, the uncontrolled high field side gas injection resulted in continuous fueling at a decreasing rate throughout a discharge, and led to detachment of the inner divertor leg at low density $\bar{n}_e \simeq (2 - 3) \times 10^{19}$ m^{-3} [35, 31] and the inner divertor MARFE formation. These factors were thought to be responsible for the monotonic density rise observed in most NBI-heated ELM-free or small ELM H-mode discharges. To achieve better density control, H-mode experiments were carried out with the reduced high field side fueling complemented by the SGI-2.

Shown in Fig. 14 are the waveforms of three 0.8 MA, 4-6 MW NBI-heated ELM-free H-mode discharges, fueled by various D$_2$ quantities from the high field side and SGI-2 injectors. The three fueling scenarios include: 1) high field side fueling at $\Gamma \simeq 40$ Torr l / s and no SGI-2; 2) reduced high field side fueling at $\Gamma \simeq 12.5$ Torr l / s and three SGI-2 pulses at $\Gamma \simeq 120$ Torr l / s; and 3) reduced high field side fueling at $\Gamma \simeq 9$ Torr l / s, one SGI-2 pulse at $\Gamma \simeq 120$ Torr l / s. Evident from the figure is a significant, 30-50 % line-averaged density reduction due to the reduced high field side injector rate. A clear density increase due to SGI-2 fueling is evident in the H-mode phase when the cases 2) and 3) are compared. Divertor D$_\alpha$ traces indicated that the high field side injection created a constant elevated recycling background. The particles injected by the SGI-2 caused a prompt build-up of the divertor density (evident from the D$_\alpha$ intensity increase).The outer midplane neutral pressure measured by a micro-ion gauge appeared to be sensitive to the high field side rate, and only weakly sensitive to the SGI-2 injection. The inner divertor pressure,
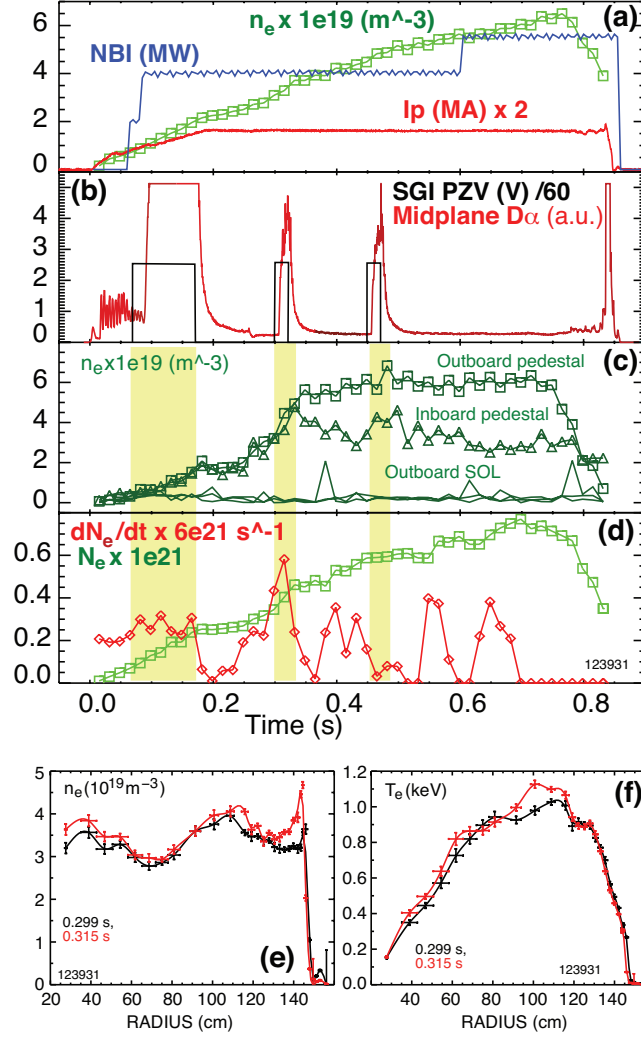
Fig. 13. Time traces of a representative SGI-2-fueled H-mode discharge: (a) Plasma current I_p, NBI power, line-averaged density $\bar{n}_e$, (b) Midplane D_α emission, SGI-2 valve control voltage, (c) Electron density measured by the Thomson scattering system in the SOL and at the H-mode pedestal (inboard and outboard), (d) Total electron inventory, and its time derivative; (e) Electron density profiles before and after the SGI-2 pulse; (f) Electron temperature profiles before and after the SGI-2 pulse.

measured by the divertor Penning gauge, followed the divertor D_α trend - it was proportional to the high field side rate, and promptly responded to the SGI-2 pulses. The observations suggest that there was a strong link between the SGI-2 fueling and divertor recycling and density. While little gas from SGI-2 was spread throughout the vacuum vessel, the injected particles were deposited in the SOL, fueled H-mode pedestal by radial plasma transport, and recycled in the divertor, building up the divertor neutral pressure and contributing to the density rise.

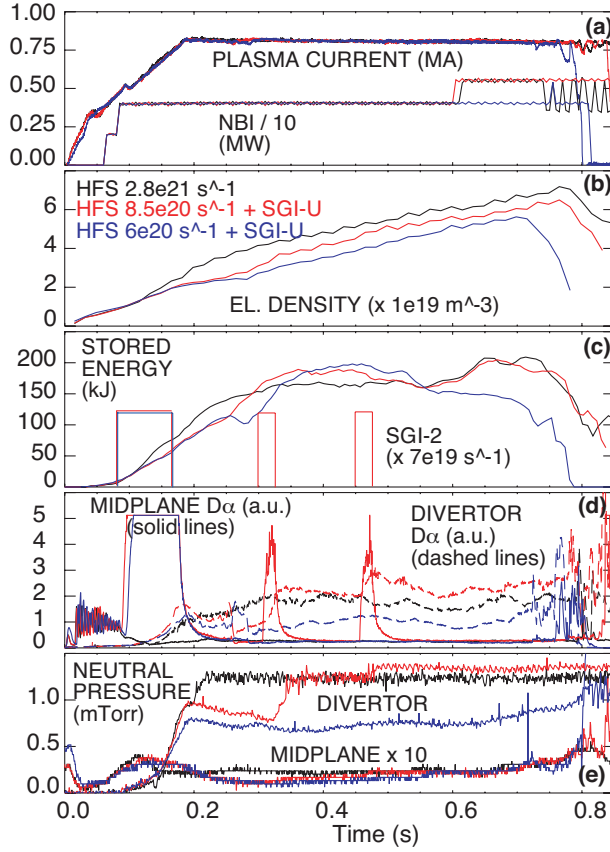We conclude this section with a note on the durability of the SGI/SGI-2 graphite nozzle.

Fig. 14. Waveforms of three H-mode discharges fueled by 1) high field side injector only (black traces), 2) reduced high field side injector rate and three SGI-2 pulses (red traces), 3) reduced high field side injector rate and one SGI-2 pulse (blue traces). (a) Plasma current, NBI heating power; (b) Electron density; (c) Plasma stored energy, SGI-2 pulses; (d) Midplane and divertor D_α intensities; (e) Midplane and divertor neutral pressures.

The SGI/SGI-2 head has been used without modifications on NSTX for six years at a moderate use rate of a few experimental days per year. By the end of this period, the nozzle edge had been eroded due to plasma-surface interactions on one side (the ion side) and had to be replaced. Fig. 15 shows a photograph of the nozzle front with the eroded exit edge. These nozzle edge modifications could have resulted in modification of the boundary layer surrounding the supersonic jet and could have potentially affected the jet characteristics in the last year of operations.

V. SUPERSONIC GAS INJECTOR CALIBRATION

Two types of calibrations have been routinely performed with the SGI/SGI-2 apparatus before and after each NSTX plasma campaign. These included a precision spatial calibration of the

Fig. 15. A photograph of the SGI nozzle eroded by plasma after six years of operation.

SGI head on the movable probe, and a gas flow (injection) rate calibration. The spatial calibration is important because the SGI is moved into the vacuum vessel for every plasma discharge when used, and moved out for helium glow discharge wall conditioning between plasma discharges. As mentioned in Sections III and IV, if the SGI head is positioned at a smaller major radius than the midplane limiter, it can overheat due to interaction with energetic particles lost from the plasma. The gas injection rate calibration is important because the SGI flow rate is controlled via the plenum pressure, and the amount of injected gas is controlled using both the plenum pressure and the pulse duration. The gas injection rate is also used in calculations of integrated fueling efficiency $\eta = (d\ N_e/dt)\Gamma_{SGI}^{-1}$. This section describes these calibrations.

The SGI head position is calibrated in respect to the tokamak major radius R. During operations, the SGI head is usually parked at $R = 1.98$ m when unused (completely withdrawn), at $R = 1.75$ m in the glow discharge cleaning mode (inside the port nipple), and at $R = 1.52 - 1.60$ m (several cm from plasma) during plasma operations. The spatial calibration is performed using a robotic arm with a precision tip that locates the SGI heat front surface with a sub-mm accuracy. The SGI head measurements are referenced to a computer measurements-based model of the NSTX vacuum vessel. Several measurements are taken to define each SGI head surface plane. The measurements are repeated for a large number of radial positions. During the calibrations, the SGI head is moved using the Thermionics drive. The calibration then consists of a linear function

connecting the number of steps of the drive counted from a home position to each radial location independently measured by the robotic arm. The calibration function parameters are entered into the EPICS interface. Shown in Fig. 16 are the examples of the SGI head measurements. These precision measurement can reveal misalignment of the SGI axis w.r.t. the radial direction up to a few degrees.

Flow rates have been also calibrated on a laboratory stand and *in-situ* on NSTX using neutral pressure gauges (Fig. 17). The flow rate is measured as an amount of gas injected per unit time. The gas flow rate is commonly expressed in Torr l / s. The amount of injected gas can be measured as $\Delta P \times V_i$, where ΔP is a neutral pressure difference due to the gas injection either in the SGI plenum of volume $V_i = V_{plenum}$, or the NSTX vacuum vessel volume $V_i = V_{NSTX}$. Both methods have inherent shortcoming. The SGI plenum pressure measured by the Sensotec sensor lacks high accuracy, while the plenum volume is known accurately $V_{plenum} = 125 - 250$ cc. The NSTX neutral pressures are measured accurately, however, the volume of NSTX vacuum vessel $V_{NSTX} = 28712$ liters may lack the required accuracy. In addition, the latter method can produce scatter in the measured flow rate due to ionization gauge calibration and different plenum pressure differentials ΔP for gas pulse lengths 5 - 300 ms used in the calibrations. It was found that during the SGI injection with the older plenum $V_{plenum} = 125$ cc, longer pulses lowered the plenum pressure and reduced the effective flow rates up to 10 %.

VI. CONCLUSIONS

In summary, a pulsed supersonic gas injector for fueling and diagnostic applications has been developed and operated successfully on NSTX. The SGI is comprised of a small Laval converging-diverging graphite nozzle, a commercial piezoelectric gas valve, and a diagnostic package, all mounted on a movable probe at a low field side midplane port location. The nozzle operated in a pulsed regime at room temperature, reservoir deuterium pressure up to 2500-5000 Torr (50-100 PSIA), flow rate up to 120-250 Torr l /s, and a measured Mach number of about 4. Experiments have demonstrated the SGI fast time response, high fueling efficiency in the range 0.1 - 0.3, and compatibility with H-mode plasmas.
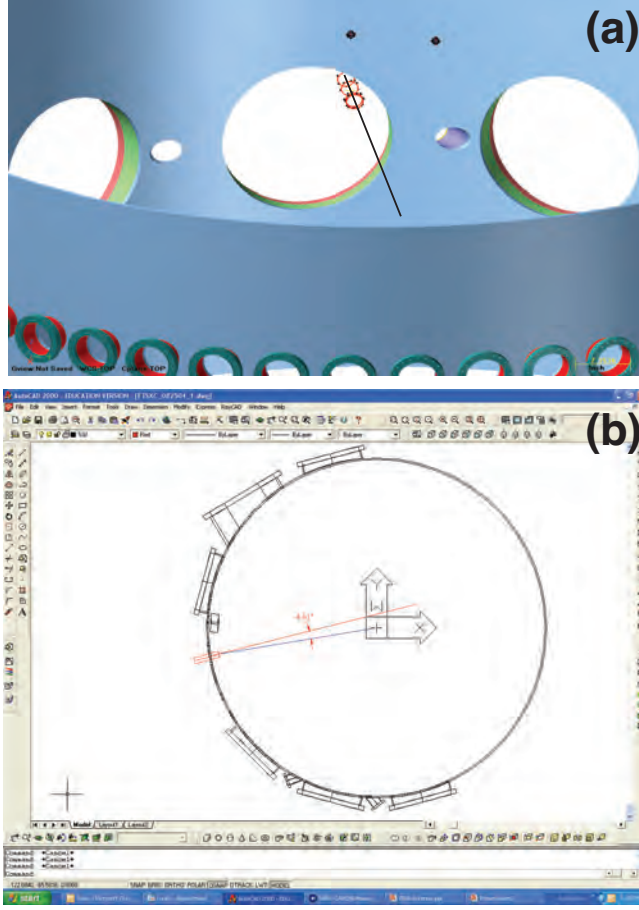
Fig. 16. Examples of AutoCAD computer drawings used in analysis of the SGI spatial calibrations: (a) the position of the SGI head w.r.t. NSTX vacuum vessel and (b) the SGI axis orientation w.r.t. NSTX radial direction.

ACKNOWLEDGMENTS

APPENDIX

A mix of pressure and volume units is used in the paper due to common use and convention. We note unit conversions for convenience.

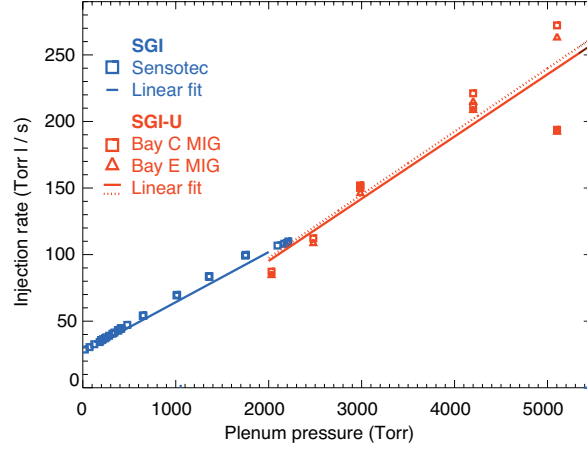Volume: $1 \text{ m}^3 = 10^6$ cubic centimiters (CC) $= 1000$ liters (l)

Fig. 17. Examples of the SGI and SGI-2 flow rate calibrations. In the SGI case, the calibration was performed using the SGI pressure drop as measured by Sensotec sensor. In the SGI-2 case, NSTX neutral pressure increase and NSTX volume were used as described in the text.

Pressure: $1 \text{ Pa} = 10^{-5} \text{ bar} = 7.5 \times 10^{-3} \text{ Torr} = 9.87 \times 10^{-6} \text{ atm} = 1.45 \times 10^{-4} \text{ PSIA}$.

Rate: $1 \text{ Pa m}^3/\text{s} = 7.5 \text{ Torr l / s} = 5.25 \times 10^{20} \text{ particles/s (D}_2)$.

REFERENCES

[1] ITER Physics Expert Group on Divertor, et. al., *Nuc. Fusion*, **39**, *12*, 2391 (1999).

[2] A. Loarte, B. Lipschultz, A. Kukushkin, G. Matthews, P. Stangeby, N. Asakura, G. Counsell, G. Federici, A. Kallenbach, K. Krieger, A. Mahdavi, V. Philipps, D. Reiter, J. Roth, J. Strachan, D. Whyte, R. Doerner, T. Eich, W. Fundamenski, A. Herrmann, M. Fenstermacher, P. Ghendrih, M. Groth, A. Kirschner, S. Konoshima, B. LaBombard, P. Lang, A. Leonard, P. Monier-Garbet, R. Neu, H. Pacher, B. Pegourie, R. Pitts, S. Takamura, J. Terry, E. Tsitrone, the ITPA Scrape-off Layer, and D. P. T. Group, "Chapter 4: Power and particle control," *Nucl. Fusion*, **47**, S203 (2007).

[3] B. Lipschultz, X. Bonnin, G. Counsell, A. Kallenbach, A. Kukushkin, K. Krieger, A. Leonard, A. Loarte, R. Neu, R. Pitts, T. Rognlien, J. Roth, C. Skinner, J. Terry, E. Tsitrone, D. Whyte, S. Zweben, N. Asakura, D. Coster, R. Doerner, R. Dux, G. Federici, M. Fenstermacher, W. Fundamenski, P. Ghendrih,

A. Herrmann, J. Hu, S. Krasheninnikov, G. Kirnev, A. Kreter, V. Kurnaev, B. Labombard, S. Lisgo, T. Nakano, N. Ohno, H. Pacher, J. Paley, Y. Pan, G. Pautasso, V. Philipps, V. Rohde, D. Rudakov, P. Stangeby, S. Takamura, T. Tanabe, Y. Yang, and S. Zhu, *Nucl. Fusion*, **47**, 1189 (2007).

[4] G. Haas, M. Keilhacker, and K. Lackner, "Comparison of different refuelling methods with respect to plasma contamination," *J. Nucl. Mater.*, **76-77**, 279 (1978); https://doi.org/10.1016/0022-3115(78)90158-7.

[5] L. Yao, N. Tang, Z. Cui, D. Xu, Z. Deng, X. Ding, J. Luo, J. Dong, G. Guo, S. Yang, C. Cui, Z. Xiao, D. Liu, X. Chen, L. Yan, D. Yan, E. Wang, and X. Deng, "Plasma behaviour with molecular beam injection in the HL-1M tokamak," *Nucl. Fusion*, **38**, *4*, 631 (1998).

[6] X. Gao, Y. Jie, C. Xia, M. Wei, Y. Yang, S. Zhang, J. Zhao, L. Hu, Y. Zhu, J. Luo, Y. Zhao, N. Qiu, J. Li, B. Wan, G. Kuang, X. Zhang, X. Liu, X. Gong, Y. Bao, B. Lin, Z. Wu, Y. Li, Y. Shi, M. Song, P. Fu, X. Zhang, M. Zeng, A. Xie, N. Cui, H. Ruan, L. Wang, B. Sheng, S. Liu, W. Ye, K. Yang, J. Liu, Y. Cheng, H. Fan, S. Liu, X. Tong, J. Mao, X. Gu, J. Xie, and Y. Wan, "High density operation on the HT-7 superconducting tokamak," *Nucl. Fusion*, **40**, *11*, 1875 (2000).

[7] B. Pégourié, E. Tsitrone, R. Dejarnac, J. Bucalossi, G. Martin, J. Gunn, D. Frigione, D. Reiter, P. Ghendrih, and C. Clément, "Supersonic gas injection on Tore Supra," *J. Nucl. Mater.*, **313-316**, 539 (2003); https://doi.org/10.1016/S0022-3115(02)01462-9.

[8] V. Soukhanovskii, H. Kugel, R. Kaita, R. Majeski, and A. Roquemore, "Supersonic gas injector for fueling and diagnostic applications on the National Spherical Torus Experiment," *Rev. Sci. Instrum.*, **75**, *10 II*, 4320 (2004).

[9] S. B. Bhatt, A. Kumar, K. Subramanian, and P. Atrey, "Gas puffing by molecular beam injection in Aditya tokamak," *Fusion Eng. Design*, **75**, 655 (2005).

[10] P. T. Lang, J. Neuhauser, J. Bucalossi, A. Chankin, D. P. Coster, R. Drube, R. Dux, G. Haas, L. D. Horton, S. Kalvin, G. Kocsis, M. Maraschek, V. Mertens,

V. Rohde, V. Rozhansky, R. Schneider, I. Senichenkov, I. Veselova, E. Wolfrum, and A. U. Team, "Impact of a pulsed supersonic deuterium gas jet on the ELM behaviour in ASDEX Upgrade," *Plasma Phys. Control. Fusion*, **47**, *9*, 1495 (2005).

[11] A. Voronin, V. Gusev, Y. Petrov, N. Sakharov, K. Abramova, E. Sklyarova, and S. Tolstyakov, "High kinetic energy plasma jet generation and its injection into the Globus-M spherical tokamak," *Nucl. Fusion*, **45**, *9*, 1039 (2005).

[12] S. Collis, J. Howard, B. D. Blackwell, P. Carlsson, M. Abelsson, and B. Powell, "A supersonic gas injection system for fuelling and probing fusion plasmas," *Plasma Sources Science and Technology*, **15**, *4*, 797 (2006).

[13] L. Yao, B. Feng, C. Chen, Z. Shi, B. Yuan, Y. Zhou, X. Duan, H. Sun, J. Lu, Y. Jiao, G. Ni, H. Lu, W. Xiao, W. Li, Y. Pan, W. Hong, H. Ran, X. Ding, and Y. Liu, "Plasma behaviour with hydrogen supersonic molecular beam and cluster jet injection in the HL-2A tokamak," *Nucl. Fusion*, **47**, *11*, 1399 (2007).

[14] H. Takenaga, Y. Miyo, J. Bucalossi, V. Marty, H. Urano, N. Asakura, T. Nishiyama, T. Sasajima, K. Masaki, and A. Kaminaga, "Fuelling characteristics of supersonic molecular beam injection in JT-60U," *Nucl. Fusion*, **50**, *11*, 115003 (2010).

[15] D. Lundberg, R. Kaita, and R. Majeski, "Molecular hydrogen density measurements of short-pulse, high-density fuelling from a molecular cluster injector," *Nucl. Fusion Fusion*, **52**, *1*, 013016 (2012).

[16] J. Kim, Y.-M. Jeon, W. Xiao, S.-W. Yoon, J.-K. Park, G. Yun, J.-W. Ahn, H. Kim, H.-L. Yang, H. Kim, S. Park, J. Jeong, M. Jung, G. Choe, W. Ko, S.-G. Lee, Y. Nam, J. Bak, K. Lee, H. Na, S.-H. Hahn, P. Diamond, T. Rhee, J. Kwon, S. Sabbagh, Y. Park, H. Park, Y. Na, W. Kim, J. Kwak, and the KSTAR contributors, "ELM control experiments in the KSTAR device," *Nucl. Fusion*, **52**, *11*, 114011 (2012).

[17] X. Zheng, J. Li, J. Hu, J. Li, R. Ding, B. Cao, and J. Wu, "Comparison between gas puffing and supersonic molecular beam injection in plasma density feedback experiments in EAST," *Plasma Phys. Control. Fusion*, **55**, *11*, 115010 (2013).

[18] H. W. Kugel et al., *J. Nuc. Mater.*, **363-365**, 791 (2007).

[19] V. A. Soukhanovskii, R. Maingi, R. Raman, H. W. Kugel, B. P. LeBlanc, A. L. Roquemore, and C. H. Skinner, "Core fueling and edge particle flux analysis in ohmically and a uxiliary heated NSTX plasmas," *J. Nuc. Mater.*, **313**, 573 (2003).

[20] H. W. Kugel et al., *Proc. 20th IEEE/NPSS Symposium on Fusion Eng.*, IEEE, San Diego, CA (2003).

[21] Y. Jiao et al., *Plasma Phys. Control. Fusion*, **45**, 2001 (2003).

[22] V. Rozhansky et al., *Nuc. Fusion*, **46**, *2*, 367 (2006).

[23] M. A. Saad, *Compressible Fluid Dynamics*, Prentice Hall, Englewood Cliffs, NJ (1993).

[24] O. F. Hagena, "Cluster ion sources (invited)," *Rev. Sci. Instrum.*, **63**, 2374 (1992).

[25] L. Yao, Y. Zhou, J. Cao, B. Feng, Z. Feng, J. Luo, J. Dong, L. Yan, W. Hong, E. Li, Z. Cui, Y. Liu, E. Wang, and J. Yan, "Hydrogen cluster-like behaviour during supersonic molecular beam injection on the HL-1M tokamak," *Nuclear Fusion*, **41**, *7*, 817 (July 2001).

[26] M. L. Baumgartner, "Turbulence Structure in a Hypersonic Boundary Layer," PhD Thesis, Princeton University (1997).

[27] (MWI, Inc, Rochester, NY 14623)URL http://www.mwi-inc.com.

[28] S. Sabbagh, S. Kaye, J. Menard, F. Paoletti, M. Bell, R. Bell, J. Bialek, M. Bitter, E. Fredrickson, D. Gates, A. Glasser, H. Kugel, L. Lao, B. LeBlanc, R. Maingi, R. Maqueda, E. Mazzucato, D. Mueller, M. Ono, S. Paul, M. Peng, C. Skinner, D. Stutman, G. Wurden, W. Zhu, and N. R. Team, "Equilibrium properties of spherical torus plasmas in NSTX," *Nucl. Fusion*, **41**, *11*, 1601 (2001).

[29] D. Johnson, N. Bretz, B. LeBlanc, R. Palladino, D. Long, and R. Parsells, "Multipulse Thomson scattering system for the National Spherical Torus Experiment," *Rev. Sci. Instrum.*, **70**, *1*, 776 (1999); 10.1063/1.1149276.

[30] B. P. LeBlanc, R. E. Bell, D. W. Johnson, D. E. Hoffman, D. C. Long, and R. W. Palladino, "Operation of the NSTX Thomson scattering system," *Rev. Sci. Instrum.*, **74**, *3*, 1659 (2003).

[31] V. SOUKHANOVSKII, R. BELL, C. BUSH, R. KAITA, H. KUGEL, B. LeBlanc, R. MAINGI, R. RAMAN, and A. ROQUEMORE, "On the secular density rises in NBI-heated H-mode plasmas in NSTX," *J. Nucl. Mater.*, **390-391**, 516 (2009).

[32] S. C. BATES and K. H. BURRELL, *Rev. Sci. Instrum.*, **55**, 934 (1984).

[33] P. SICHTA and J. DONG, *Proc. 19th IEEE/NPSS Symposium on Fusion Eng.*, 245, IEEE, Atlantic City, NJ (2002).

[34] R. MAINGI, C. S. CHANG, S. KU, T. BIEWER, and R. MAQUEDA, *Plasma Phys. Control. Fusion*, **46**, A305 (2004).

[35] V. SOUKHANOVSKII, R. MAINGI, A. ROQUEMORE, J. BOEDO, C. BUSH, R. KAITA, H. KUGEL, B. LEBLANC, S. PAUL, G. PORTER, and N. WOLF, "Divertor regimes in NSTX," *J. Nucl. Mater.*, **337-339**, *1-3*, 475 (2005).